Anomalously Large Chiral Sensitivity in the Dissociative Electron Attachment of 10-Iodocamphor

J. M. Dreiling,[1,*] F. W. Lewis,[2] J. D. Mills,[3] and T. J. Gay[1]
[1]Jorgensen Hall, University of Nebraska, Lincoln, Nebraska 68588-0299, USA
[2]Department of Applied Sciences, Faculty of Health and Life Sciences, Northumbria University, Newcastle upon Tyne, NE1 8ST, United Kingdom
[3]Air Force Research Laboratory, Aerospace Systems Directorate, Propellants Branch, AFRL/RQRP, Edwards AFB, California 93524, USA

(Received 1 October 2015; revised manuscript received 30 December 2015; published 3 March 2016)

We have studied dissociative electron attachment (DEA) between low energy (≤ 0.6 eV) longitudinally polarized electrons and gas-phase chiral targets of 3-bromocamphor ($C_{10}H_{15}BrO$), 3-iodocamphor ($C_{10}H_{15}IO$), and 10-iodocamphor. The DEA rate depends on the sign of the incident electron helicity for a given target handedness, and it varies with both the atomic number (Z) and location of the heaviest atom in the molecule. While simple dynamic mechanisms can account for the asymmetry dependence on Z, they fail to explain the large asymmetry variation with the heavy atom location.

DOI: 10.1103/PhysRevLett.116.093201

When longitudinally polarized (chiral) electrons scatter from unoriented chiral molecules, scattering cross sections for the various collision channels generally depend on the handedness of the collision constituents [1,2]. Such dependence has the mechanical analog of the ability of, e.g., left-handed nuts to be threaded onto left-handed but not right-handed bolts. Chiral asymmetries were first observed in gas-phase electron-molecule collisions by the Münster group in 1995 for quasielastic scattering [3–5] (but, see also Refs. [6,7]). A number of interesting experiments done since then have involved the transmission of polarized electrons through solid chiral films [8–10]. Recently, we reported the observation of chiral asymmetries in a gas-phase resonant interaction–dissociative electron attachment (DEA):

$$e^- + AB \rightarrow A + B^-, \tag{1}$$

where AB is a generic two-component molecule. In our work, we used bromocamphor ($C_{10}H_{15}BrO$) and monitored the production of Br anions [11]. The observation of chiral sensitivity in a breakup reaction is important because, among other things, it validates the premise of the Vester-Ulbricht hypothesis regarding the origins of biological homochirality [12]. More generally, such low-energy interactions play a crucial role in processes such as, e.g., electron-induced damage of biomolecules [13].

While symmetry permits the existence of chiral sensitivity in such unoriented gas phase experiments, its dynamic causes are poorly understood [14–17]. To our knowledge, there exist no *ab initio* calculations of these effects. Nonzero asymmetries in a given scattering channel might result from one or more qualitatively different dynamic mechanisms involving (a) continuum Mott scattering, (b) spin-other-orbit coupling between the incident electron and the magnetic moment it induces in the chiral target, and (c) nonzero average helicity of the target electrons [14,16]. (In this Letter, we will refer to these as Mott scattering, spin-other-orbit coupling, and helicity density, respectively.)

We consider these mechanisms in turn in a semiclassical way, as they pertain to DEA (Fig. 1). The DEA reaction requires that the incident electron form a temporary negative molecular ion that dissociates, unless autodetachment occurs first [18]. The electron density associated with this state is typically localized in the vicinity of the atom(s) that will ultimately form the ionic fragment.

A Mott-scattering mechanism [Fig. 1(a)] [2,16] would involve first a primarily Coulombic scattering from a light atom that turns the incident electron's longitudinal spin into a transverse one. Subsequent Mott scattering from the target's heaviest atom (atomic number Z) leads to asymmetric scattering of the two possible spin directions. Averaged over all target orientations, this would favor, e.g., the spin-forward electrons in setting up a resonant state in the vicinity of the high-Z atom. Because of the target's

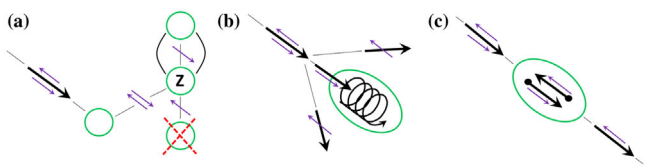

FIG. 1. Schematic diagrams of collisional mechanisms leading to chiral asymmetries, showing (a) Mott scattering with a DEA precursor resonant state indicated by curved lines, (b) spin-other-orbit coupling, and (c) helicity density (see text). Heavy and light arrows indicate electronic momenta and spins, respectively. Incident electrons arrive from the upper left.

chiral geometry, the spin-backward electron will more often lack a scattering center as it exits the target volume; this is depicted by the crossed-out atom in Fig. 1(a). The asymmetry associated with this mechanism depends on Z^2.

In the spin-other-orbit coupling mechanism [16,19], which comprises the dynamics that cause optical activity and photonic circular dichroism, the electromagnetic impulse from the incident electron induces a helical current in the target, producing a magnetic dipole moment [Fig. 1(b)]. The spin of the incident electron would interact differently with this dipole depending on whether it is forward or backward. Thus, e.g., spin-backward electrons would be scattered away from the target more than those with spin forward, inhibiting the ability of the former to set up a DEA precursor resonant state. Such coupling would have no explicit Z dependence, although it would tend to be correlated with the total atomic weight of the molecule, to the extent that this value is associated with the target's polarizability.

Finally, electrons in chiral molecules have nonzero average helicity [16,20–22]. One would thus expect that a DEA precursor state with, e.g., a positive helicity density would be more likely to be populated by spin-forward (positive helicity) electrons than by spin-backward ones [Fig. 1(c)]. Such asymmetries are also expected to scale like Z^2.

No experiment done to date has given a clear picture of the relative importance of the above three mechanisms in determining chiral asymmetries. These mechanisms apply also to the quasielastic transmission of spin-polarized electrons through chiral molecules [16]. Chiral sensitivity of total cross sections has been observed with gas-phase targets only if $Z \geq 35$ [3–5]. This argues circumstantially for the importance of either a Mott scattering or helicity-density mechanism but against spin-other-orbit coupling. In contrast, the electron transmission studies done with camphor-lanthanoid complexes having a variation in Z^2 from 3481 to 4900 had no obvious Z dependence [5,14,16]. This situation, combined with the paucity of *ab initio* gas-phase theory, illustrates our poor current understanding of even the most qualitative aspects of electron-chiral molecule interactions.

This Letter describes measurements of chiral asymmetries for halocamphor targets in the gas phase in which we have tried to clarify the role the above mechanisms play. To this end, we varied Z^2 from 1225 (Br) to 2809 (I) and changed the position of the heavy atom within the molecule to probe the role of its proximity to a chiral center. Our apparatus [11] has four main components: an active-feedback optical system, a polarized electron source, a target chamber, and an optical electron polarimeter. The source of longitudinally spin-polarized electrons is a GaAs photocathode [23]. The optical setup used to produce the circularly polarized light for photoemission also allows for active feedback to reduce instrumental asymmetries [24].

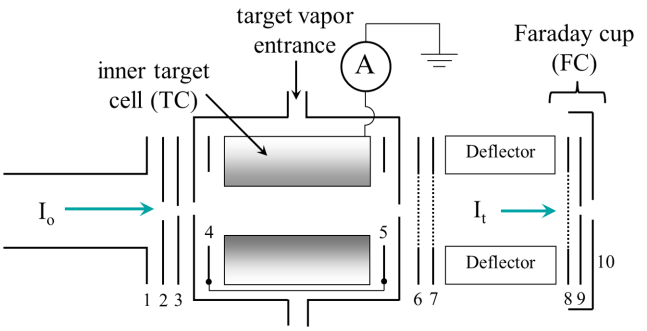

FIG. 2. Detail of the target vapor cell, showing the incident (I_o) and transmitted (I_t) electron beams, the target cell structure, and the Faraday cup assembly used to measure I_t. Electrostatic lens elements, retarding-field meshes, and apertures are also shown.

Following extraction from the source, the electron beam is magnetically guided to the target (see Fig. 2), which is kept at ~80 °C to prevent condensation of halocamphor vapor on the electron-optical elements. The electron beam transmitted through the target vapor is detected as a current on the Faraday cup (FC). We measure the electron polarization using optical polarimetry [16]; it is typically ~30%.

During an asymmetry measurement, molecules of a given handedness were admitted to the target cell until the electron beam transmitted to the FC at 0 V target retarding voltage was attenuated by 50%. This corresponded to a pressure of 0.5–1.5 mTorr as measured by a capacitance manometer and required the samples to be heated to a temperature of 50–60 °C. The reduction in current is associated with the total cross section of the target and corresponds to multiple electron-molecule interactions including, but not limited to, DEA, quasielastic scattering, and vibrational excitation. A 15 mT longitudinal magnetic field guided scattered electrons out of the target cell, while the anions, due to their larger mass, were able to cross the magnetic field lines and be detected as a current on the isolated inner target cell walls. Electron-spin-dependent asymmetries were determined using a lock-in amplifier to detect the change in target-cell-wall current at the frequency of the electron helicity reversal. Checks of our measurements [11,25] confirmed our ability to measure chirally dependent asymmetries less than 10^{-4}, validated our detection of a negative ion current from DEA, and provided an upper limit of $\leq 20\%$ (and, more typically, $< 8\%$) for scattered-electron contributions to the DEA signal.

For a measurement with a given target handedness, the electron helicity was reversed at a frequency of ~210 Hz, and the DEA current asymmetry associated with the helicity reversal,

$$a_{+(-)} = \left[\frac{I\uparrow - I\downarrow}{I\uparrow + I\downarrow}\right]_{+(-)}, \tag{2}$$

was monitored for about 3 min. Here, $I\uparrow$ ($I\downarrow$) is the target-cell-wall current for spin-forward (spin-backward) electrons, and the + and − subscripts denote the molecular handedness. The target chirality was then switched and data collected again. A final asymmetry value, A, was calculated using

$$A = a_- - a_+ = \left[\frac{I\uparrow - I\downarrow}{I\uparrow + I\downarrow}\right]_- - \left[\frac{I\uparrow - I\downarrow}{I\uparrow + I\downarrow}\right]_+ . \quad (3)$$

At each voltage, A was measured ∼10 times, and an average was found after applying Chauvenet's criterion [26]. Data were taken using two orthogonal settings of the quarter-wave plate that circularly polarizes the source laser light, thereby flipping the sign of the electron polarization for a given optical configuration [24]. Uncertainties were determined by taking the quadrature sum of the statistical counting uncertainty (given by the standard deviation of the mean of the measurements at a given energy) and the systematic error (estimated by the magnitude of the sum of the measurements with opposite quarter-wave plate settings).

Figure 3 shows the DEA asymmetry for the molecules we investigated through a range of electron energies near 0 eV. To explore the effect of Z on A, we compared our

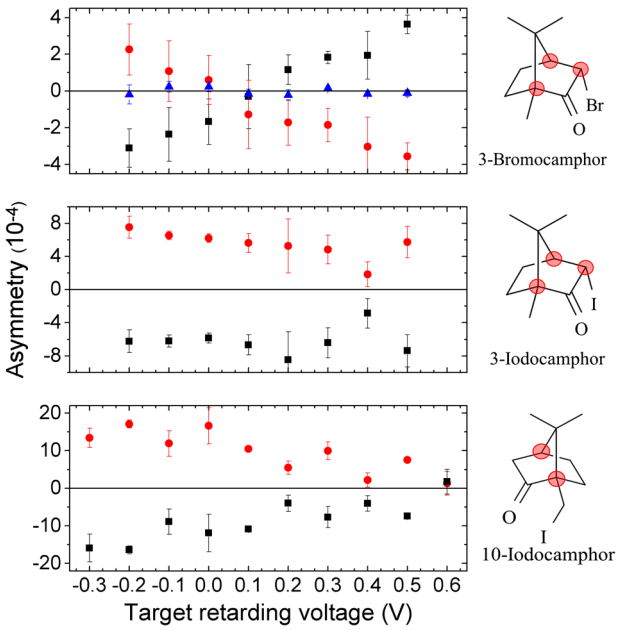

FIG. 3. The asymmetry, A, in DEA current as a function of target retarding voltage for each halocamphor compound, whose (+) enantiomers are shown at the right with chiral centers indicated. Squares and circles represent opposite settings of the quarter-wave plate that circularly polarizes the laser light, which should give asymmetry measurements of opposite signs. The triangles indicate data taken with a racemic mixture of bromocamphor. Uncertainties are described in the text except for those of the racemic data, which are purely statistical.

previously-measured asymmetries for 3-bromocamphor (referred to below as 3Br for brevity) [11] with those of 3-iodocamphor (3I). Additionally, we studied the effect of constitution on the chiral asymmetry by investigating the constitutional isomer 10-iodocamphor (10I). The iodocamphor molecules used in this study were synthesized as discussed in the Supplemental Material [27].

In Fig. 3, a null target retarding voltage corresponds to the peak in the derivative of the current transmitted to the FC with no target gas [25]. The derivative curve was quasi-Gaussian with a width of ∼0.6 eV, which is an upper limit of the incident beam's energy width. The average incident electron kinetic energy in the target varies monotonically but non-linearly with the retarding potential. The beam's energy width also increases monotonically with target retarding voltage, varying from $\lesssim$0.15 eV at −0.3 V to $\lesssim$0.6 eV at 0.6 V.

The data for each target differ both in their maximum absolute values and their dependence on incident electron energy. The maximum asymmetries, $A_{\max}$, for 3Br, 3I, and 10I are roughly 4×10^{-4}, 8×10^{-4}, and 16×10^{-4}, respectively. The 3Br asymmetries completely reverse their sign over the energy range investigated. The 3I data exhibit a possible energy-dependent feature at 0.4 V; the 10I asymmetry magnitudes have a slow overall decrease with increasing energy and possibly significant features across the energy range. We note that the 3I data have a ∼10% contamination of *exo*-stereoisomers, and the iodine in the 10I targets has an average position distributed in accord with the halomethyl torsional degree of freedom.

We now consider our DEA results in terms of the three models for the production of chiral asymmetries discussed above. Our 3Br and 3I data provide clear evidence for Z dependence in the DEA channel. The values of $A_{\max}$ for 3I and 10I are both significantly larger than those for 3Br, and, in the case of equivalent molecular structure, the difference scales qualitatively as Z^2. The Z dependence we observe in the DEA channel argues for either Mott scattering or helicity density being responsible for the chiral sensitivity. Such Z dependence is not expected for spin-other-orbit effects. Indeed, measurements of optical rotatory power for the Na D line at 589 nm, which is caused by dynamics of this type, indicate specific rotations of 131°, 147°, 24.8°, and 21.2° for 3Br, 3I, 10Br, and 10I, respectively [30–33].

We expect Mott scattering to be most important if the high-Z atom responsible for the internal scattering asymmetries is directly attached to a chiral center. But for 10I, $A_{\max}$ is twice that observed with 3I, even though the iodine in 3I is directly attached to a chiral center, while the 10I iodine atom is separated by two bonds from the nearest chiral center. Mott scattering would thus not appear to be the primary mechanism creating these DEA asymmetries.

We are thus led to consider helicity density to explain the Z dependence. To this end, we calculated the helicity density as a function of position, $h(\vec{r})$, for the ground states

of 3Br, 3I, and 10I. Based on similar previous work [14,22], we employed conventional restricted-Hartree-Fock calculations to optimize geometries using the GAMESS quantum chemical suite [34] with a 6-31G(d) basis for 3Br [35] and the DZP basis for 3I and 10I [36]. For 3Br and 3I, the *endo*-isomer was calculated. For 10I, $h(\vec{r})$ was determined for the structures corresponding to the three local torsional minima of the halomethyl group, all lying within 0.11 eV of each other. As singlet-triplet mixing due to spin-orbit interaction is responsible for the helicity density in our model [20], we performed a standard, first-order perturbation calculation to assess the degree of triplet contamination of the ground state for the various geometries we considered. The MINI basis [37] was used with a development version of the CRUNCH code suite [38].

The calculated helicity density parameters are presented in Table I and discussed in what follows. The expectation value of the helicity operator, or the "electronic helicity," H, is obtained by integrating $h(\vec{r})$ over the entire molecular volume [14]. However, in DEA, it seems likely that the sign and magnitude of the helicity density is important only in the vicinity of the carbon-halogen (C-X) bond. We thus integrated $h(\vec{r})$ within the region of an ellipsoid with the carbon and the halogen atoms at the foci and a ratio of 0.7 between the minor and major axes. This yields the "bond helicity," H_b.

Finally, we consider in more detail the resonant nature of DEA in a helicity density picture. In its simplest form, DEA of the halocamphors involves the incident electron populating a low-lying (normally) unoccupied molecular orbital associated with the C-X bond. Halogen anions are produced if these orbitals are antibonding. Another possibility exists; the lowest orbitals may have mixed character, distributing themselves across both the C-X and C-O carbonyl bonds. The carbonyl component is of local π^* character and has a relatively long lifetime. One might expect that a longer-lived resonance would result in higher DEA chiral asymmetries, since the electron has a better chance to "sample the target's chirality" [39] and could subsequently leak from the molecule's carbonyl bond to the C-X antibonding region. We can estimate the viability of these mechanisms by integrating the product of $h(\vec{r})$ and the electronic density of the two lowest unoccupied molecular orbitals (LUMO and LUMO + 1) in turn over the bond ellipsoid, giving the "LUMO (LUMO + 1)-weighted bond helicity," H_L (H_{L+1}). For 3Br and 3I, these two orbitals have predominantly σ^* antibonding character in the C-X region, combined with significant carbonyl π^* character. For 10I, only the LUMO exhibits antibonding characteristics in the C-X region; the LUMO + 1 has almost no density there. These qualitative spatial considerations are born out quantitatively in the values we have calculated for H_L and H_{L+1}.

TABLE I. Calculated helicity density parameters: electronic helicity, H; bond helicity, H_b; LUMO-weighted bond helicity, H_L; LUMO + 1-weighted bond helicity, H_{L+1}; and maximum observed asymmetry $A_{\max}$. All helicity values are reported in units of $\alpha^2/2$.

Molecule	H	H_b	H_L	H_{L+1}	$A_{\max}(10^{-4})$
3Br	−15.6	1.48	0.05	0.14	4
3I	−19.9	5.32	0.23	0.22	8
10I	−1.9	−0.44	−0.01	N/A	16

All our helicity density calculations imply strongly that chiral asymmetries ought to be far smaller for 10I than for our other two targets, but the opposite is true. We are thus forced to exclude this mechanism as the main cause of these asymmetries as well. While it is possible that spin-other-orbit coupling could account for this result, it seems unlikely given its lack of explicit Z dependence and the clear-cut nuclear charge effects observed in the 3-halocamphors. Mott scattering can possibly account for our results in 3Br and 3I, but neither Mott scattering nor a helicity density picture accounts for the particularly large chiral sensitivity seen in 10I.

We note a correlation between $A_{\max}$ of a given target and the mean electron kinetic energy where the DEA signal peaks. These occur at target retarding voltages of 0.0, +0.1, and +0.2 V, for 3Br, 3I, and 10I, respectively. (The normalized target cell current varied $< 25\%$ between all three molecules, indicating comparable DEA cross sections.) In a simple picture, higher attachment energy corresponds to a longer lifetime of the temporary molecular anion before the dissociative channel is stabilized against autoionization [18]. Since a longer lifetime could reasonably be expected to give larger chiral sensitivity based on the sampling argument discussed above, this could explain the enhanced 10I asymmetry we observe. Unfortunately, this picture is incomplete without a detailed *ab initio* calculation of the DEA dissociation dynamics, including the diabatic couplings of the relevant molecular curves. Such information is not currently available.

This investigation provides surprising new results, but little clear understanding of the dynamic mechanisms responsible for chiral asymmetry in electron-molecule collisions. We have shown that qualitative, semiclassical models fail to explain the gross features of the chiral asymmetries we observe; our attempts to quantify the helicity-density mechanism with calculations of electronic helicity parameters have not significantly improved our insight. This work thus points out the need for the development of fundamental quantum-dynamic calculations to provide a first, rudimentary understanding of the magnitudes and energy dependence of the asymmetries we observe. Even a qualitative theoretical picture of such effects would significantly improve our understanding of other, related areas such as low-energy electron-induced damage of biomolecules.

The authors would like to thank G. A. Gallup (deceased) and P. D. Burrow for enlightening discussions. We also thank Northumbria University for awarding an Anniversary Research Fellowship to F. W. Lewis. This work was funded by the U.S. National Science Foundation, Grant Nos. PHY-1206067 and PHY-1505794.

*Present address: National Institute of Standards and Technology (NIST), 100 Bureau Drive, Gaithersburg, Maryland 20899, USA.
jmdreiling2@gmail.com

[1] P. S. Farago, J. Phys. B **14**, L743 (1981).
[2] J. Kessler, J. Phys. B **15**, L101 (1982).
[3] S. Mayer and J. Kessler, Phys. Rev. Lett. **74**, 4803 (1995).
[4] S. Mayer, C. Nolting, and J. Kessler, J. Phys. B **29**, 3497 (1996).
[5] C. Nolting, S. Mayer, and J. Kessler, J. Phys. B **30**, 5491 (1997).
[6] D. M. Campbell and P. S. Farago, Nature (London) **318**, 52 (1985).
[7] K. W. Trantham, M. E. Johnston, and T. J. Gay, J. Phys. B **28**, L543 (1995).
[8] K. Ray, S. P. Ananthavel, D. H. Waldeck, and R. Naaman, Science **283**, 814 (1999).
[9] R. A. Rosenberg, M. Abu Haija, and P. J. Ryan, Phys. Rev. Lett. **101**, 178301 (2008).
[10] B. Göhler, V. Hamelbeck, T. Z. Markus, M. Kettner, G. F. Hanne, Z. Vager, R. Naaman, and H. Zacharias, Science **331**, 894 (2011), and references therein.
[11] J. M. Dreiling and T. J. Gay, Phys. Rev. Lett. **113**, 118103 (2014).
[12] F. Vester, T. L. V. Ulbricht, and H. Krauch, Naturwissenschaften **46**, 68 (1959); T. L. V. Ulbricht and F. Vester, Tetrahedron **18**, 629 (1962).
[13] B. Boudaffa, P. Cloutier, D. Hunting, M. A. Huels, and L. Sanche, Science **287**, 1658 (2000).
[14] A. M. Scheer, G. A. Gallup, and T. J. Gay, J. Phys. B **39**, 2169 (2006).
[15] A. M. Scheer, G. A. Gallup, and T. J. Gay, J. Phys. Chem. A **112**, 4029 (2008).
[16] T. J. Gay, in *Advances in Atomic, Molecular, and Optical Physics*, edited by E. Arimando, P. R. Berman, and C. C. Lin (Academic Press, Burlington, 2009), Vol. 57, p. 157.
[17] K. Blum and D. G. Thompson, in *Advances in Atomic, Molecular and Optical Physics*, edited by B. Bederson and H. Walther (Academic Press, New York, 1997), Vol. 38, p. 39.
[18] L. G. Christophorou, D. L. McCorkle, and A. A. Christodoulides, in *Electron-Molecule Interactions and Their Applications*, edited by L. G. Christophorou (Academic, Orlando, 1984), p. 477.
[19] D. W. Walker, J. Phys. B **15**, L289 (1982).
[20] A. Rich, J. Van House, and R. A. Hegstrom, Phys. Rev. Lett. **48**, 1341 (1982).
[21] R. A. Hegstrom, Nature (London) **297**, 643 (1982).
[22] G. A. Gallup, in *Electron Collisions with Molecules, Clusters, and Surfaces*, edited by H. Ehrhardt and L. A. Morgan (Plenum, New York, 1994), p. 163.
[23] D. T. Pierce, R. J. Celotta, G.-C. Wang, W. N. Unertl, A. Galejs, C. E. Kuyatt, and S. R. Mielczarek, Rev. Sci. Instrum. **51**, 478 (1980).
[24] J. M. Dreiling, S. J. Burtwistle, and T. J. Gay, Appl. Opt. **54**, 763 (2015).
[25] J. M. Dreiling and T. J. Gay, J. Phys. Conf. Ser. **635**, 012015 (2015).
[26] P. R. Bevington and D. K. Robinson, *Data Reduction and Error Analysis for the Physical Sciences* (McGraw Hill, New York, 1992), p. 58.
[27] See Supplemental Material at http://link.aps.org/supplemental/10.1103/PhysRevLett.116.093201, which includes Refs. [28,29], for more information regarding the synthesis of 3- and 10-iodocamphor.
[28] C. R. Kaiser, R. Rittner, and E. A. Basso, Magn. Reson. Chem. **32**, 503 (1994).
[29] S. Oae and H. Togo, Bull. Chem. Soc. Jpn. **56**, 3802 (1983).
[30] F. W. Lewis, G. Egron, and D. H. Grayson, Tetrahedron: Asymmetry **20**, 1531 (2009).
[31] C. Djerassi, J. Osiecki, R. Riniker, and B. Riniker, J. Am. Chem. Soc. **80**, 1216 (1958).
[32] J. P. Mathieu and J. Perrichet, C.R. Hebd. Seances Acad. Sci. **200**, 1583 (1935).
[33] J. E. H. Buston, I. Coldham, and K. R. Mulholland, J. Chem. Soc., Perkin Trans. 1 2327 (1999).
[34] M. Gordon and M. W. Schmidt, in *Theory and Applications of Computational Chemistry: The First Forty Years*, edited by C. E. Dykstra, G. Frenking, K. S. Kim, and G. E. Scuseria (Elsevier, Amsterdam, 2005), p. 1167.
[35] M. M. Franci, W. J. Pietro, W. J. Hehre, J. S. Binkley, M. S. Gordon, D. J. DeFrees, and J. A. Pople, J. Chem. Phys. **77**, 3654 (1982).
[36] A. C. Neto, E. P. Muniz, R. Centoducatte, and F. E. Jorge, J. Mol. Struct. (Theochem) **718**, 219 (2005); C. L. Barros, P. J. P. de Oliveira, F. E. Jorge, A. C. Neto, and M. Campos, Mol. Phys. **108**, 1965 (2010).
[37] S. Huzinaga, J. Andzelm, M. Klobukowski, E. Radzio-Andzelm, Y. Sakai, and H. Tatewaki, *Gaussian Basis Sets for Molecular Calculations* (Elsevier, Amsterdam, 1984).
[38] http://sourceforge.net/projects/molcrunch.
[39] T. M. Stephen, X. Shi, and P. D. Burrow, J. Phys. B **21**, L169 (1988).